Separation-enrichment method for airborne disease spores based on microfluidic chip

Yafei Wang[1,2], Xiaodong Zhang[1,2], Ning Yang[3], Guoxin Ma[1,2], Xiaoxue Du[1,2], Hanping Mao[1,2*]

(1. *School of Agricultural Engineering, Jiangsu University, Zhenjiang 212013, Jiansu, China*;
2. *Key Laboratory of Modern Agricultural Equipment and Technology, Ministry of Education, Jiangsu University, Zhenjiang 212013, Jiangsu, China*;
3. *School of Electrical and Information Engineering, Jiangsu University, Zhenjiang 212013, Jiangsu, China*)

Abstract: Airborne diseases are likely to cause crop yield reduction, which has aroused widespread concern. In this study, a two-stage separation-enrichment structure microfluidic chip with a compound field for separation and enrichment of the greenhouse crops airborne disease spores directly from gas flow was developed. The chip is mainly composed of three parts: arc structure pretreatment channel, semicircular electrode structure and collection tank. COMSOL 5.1 software was used to simulate the designed microfluidic chip. 30 μm particles were used to represent *P. xanthii* spores, 25 μm particles were used to represent *P. cubensis* spores, and 16 μm particles were used to represent *B. cinerea* spores. The simulation results showed that the separation and enrichment efficiency of 16 μm particles, 25 μm particles, and 30 μm particles was 88%, 91%, and 94%, respectively. The experimental verification results were observed under a microscope. The results showed that the separation and enrichment efficiency of *B. cinereal* spores, *P. cubensis* spores and *P. xanthii* spores was 75.7%, 83.8% and 89.4%, respectively. As a result, the designed microfluidic chip can be used to separate and enrich the spores of airborne diseases of greenhouse crops, which can provide a basis for the research of real-time monitoring technology for greenhouse airborne diseases.

Keywords: greenhouse, crop disease, airborne spore, microfluidic chip
DOI: 10.25165/j.ijabe.20211405.6375

Citation: Wang Y F, Zhang X D, Yang N, Ma G X, Du X X, Mao H P. Separation-enrichment method for airborne disease spores based on microfluidic chip. Int J Agric & Biol Eng, 2021; 14(5): 199–205.

1 Introduction

With the continuously increasing global population, the demand for the 'vegetable basket' project has increased. At present, the vegetable industry is developing rapidly in China, with a greenhouse cultivation area of more than 4 million hm^2, the largest in the world in terms of total area[1,2]. The environment in the greenhouse is conducive to the occurrence of airborne diseases, such as tomato gray mold (*Botrytis cinerea*), cucumber downy mildew (*Pseudoperonospora cubensis*), and cucumber powdery mildew (*Podosphaera xanthii*). When airborne diseases occur, with a yield loss of 20%-50%, or even no harvest[3-5]. Therefore, accurate and timely monitoring of airborne disease spores is very important.

At present, the detection methods of fungal spores mainly include image processing[6,7], weighing method[8], and polymerase chain reaction (PCR)[9,10]. However, due to the presence of a large amount of impurity, the above methods are limited in the detection of fungal spores. Therefore, it is necessary to separate and enrich the spores to improve detection accuracy. Different types of crop fungal spores have different shapes and sizes. For example, *B. cinerea* spores are almost oval and have a size distribution of 11.4-26.7 μm, *P. cubensis* spores are lemon shape and the size distribution is 21.1-39.8 μm, *P. xanthii* spores are cylindrical and the size distribution is 30.2.1-39.5 μm. There are other objects defined as impurities in the actual detection environment, and their size is less than 10 μm.

Microfluidics is a science that studies precise control and manipulation of fluids through microchannels with dimensions of tens to hundreds of micrometers and the technology of manufacturing microminiaturized devices through which fluid flow is studied. Its numerous applications cover engineering, biological, biochemistry, nanotechnology, and many systems in which small volumes of fluids are processed to achieve high-throughput screening. Microfluidics has the potential to manipulate bioparticles aimed at focusing, trapping, separating, and sorting particles[11-13]. Wang et al.[14] designed a microfluidic chip that can directly enrich airborne fungal spores from airflow. The chip includes three parts: half-wave pretreatment channel, inertial impactor and low-pressure collection chamber. Yang et al.[15] designed a microfluidic chip to capture and detect rice disease spores and realize early monitoring of crop diseases. Although,

Received date: 2020-12-25 **Accepted date:** 2021-07-07
Biographies: Yafei Wang, PhD candidate, research interest: intelligent agricultural equipment and technology, Email: wangyafei@126.com; **Xiaodong Zhang**, PhD, Associate Researcher, research interest: intelligent agricultural equipment and technology, Email: zxd700227@126.com; **Ning Yang**, PhD, Professor, research interest: intelligent agricultural equipment and technology, Email: yangning7410@163.com; **Guoxin Ma**, PhD candidate, research interest: intelligent agricultural equipment and technology, Email: Gavin_Ma123@163.com; **Xiaoxue Du**, PhD candidate, research interest: intelligent agricultural equipment and technology, Email: 2111916004@stmail.ujs.edu.cn.
***Corresponding author: Hanping Mao**, PhD, Professor, research interest: modern agricultural equipment and the Environmental control technology of facility agriculture. Department of agricultural equipment, Jiangsu University, Zhenjiang 212013, Jiangsu, China. Email: maohpujs@163.com.

the above research results can enrich and separate fungal spores in the air. However, fungal spores with similar shapes cannot be separated. Spores will be polarized under the action of a non-uniform electric field and move under the action of the electric field force. This phenomenon is called dielectrophoresis (DEP)[16]. DEP has been utilized widely for biomedical applications[17,18]. Over recent years, DEP is a non-invasive method that provides high-precision and high-efficiency analysis, which has attracted more and more attention. Zhang et al.[19] designed a DEP microfluidic chip to achieve the separation of platelets and red blood cells. Zhang et al.[20] presented a method based on DEP to rapidly separate and purify macrophages from micro-volume samples using a microfluidic device for liquid biopsy and point-of-care testing. Lee et al.[21] designed a microfluidic device for continuous separation of nanoparticles by combining diffusiophoresis and electrophoresis to achieve the separation of nanoparticles having different sizes, in order to achieve high separation performance. Notwithstanding, many studies have been conducted on particles separation on microfluidic chip based on dielectrophoretic force. To the scrutiny of the current references, however, the separation of greenhouse crops airborne disease spore using DEP technique at a microfluidic device with the continuous flow has not yet been reported.

Hence, in this study, a two-stage separation-enrichment structure microfluidic chip with a compound field for separation and enrichment of the greenhouse crops airborne disease spores directly from gas flow was developed. It can separation-enrichment of greenhouse crops airborne disease spore and achieve timely monitoring of airborne diseases.

2 Materials and methods

2.1 Theory and working principle

The proposed microfluidic device's mathematical model is presented in this part; it is based on assumptions that are listed in the literature [22]. The model consists of the equations of motion, Navier–Stokes equation, continuity equation and electric field equation. The equations of motion are provided as follows[23]:

$$m_e \frac{\mathrm{d}^2}{\mathrm{d}t^2} x_e = \sum F_{ext} \tag{1}$$

where, t is the particle motion time, s; m_e is the micro-scale entity's mass, kg; x_e is the micro-scale entity's displacement, m; F_{ext} is the external forces acting on the micro-scale entity. The inertial force associated with the micro-scale entity is presented on the left-hand side of Equation (1). The external forces to which a micro-scale entity is subjected are that due to gravity, drag, buoyancy, and DEP.

DEP refers to the movement of a polarizable particle in response to the interactions between the induced dipole moment of the particle and the spatially non-uniform electric field[24]. When a particle of radius r suspended in the medium is subjected to a non-uniform electric field E, the averaged DEP force (F_{DEP}) acting on the spores is defined as[25,26]

$$F_{\text{DEP}} = 2\pi\varepsilon_m r^3 \operatorname{Re}[K^*(\omega)]\nabla(|E|^2) \tag{2}$$

where, r is the radius of the particle, μm; ε_m is the permittivity of the medium; ∇ is the gradient operator. $\omega=2\pi f$ is the angular frequency. $\operatorname{Re}[K^*(\omega)]$ is the real part of the complex Claussius-Mossotti (CM) factor[27,28], which is given by

$$\varepsilon^* = \varepsilon - \frac{j\sigma}{\omega} \tag{3}$$

$$\sigma^* = \sigma + j\omega\varepsilon_0\varepsilon \tag{4}$$

$$K^*(\omega) = \frac{\varepsilon_p^* - \varepsilon_m^*}{\varepsilon_p^* + 2\varepsilon_m^*} = \frac{(\varepsilon_p - \varepsilon_m) + j\dfrac{\sigma_m - \sigma_p}{\omega}}{(\varepsilon_p + 2\varepsilon_m) - j\dfrac{2\sigma_m + \sigma_p}{\omega}} \tag{5}$$

$$\operatorname{Re}[K^*(\omega)] = \operatorname{Re}\left(\frac{\varepsilon_p^* - \varepsilon_m^*}{\varepsilon_p^* + 2\varepsilon_m^*}\right) = \frac{\omega^2(\varepsilon_p - \varepsilon_m)(\varepsilon_p + 2\varepsilon_m) + (\sigma_p - \sigma_m)(2\sigma_m + \sigma_p)}{\omega^2(\varepsilon_p + 2\varepsilon_m)^2 + (2\sigma_m + \sigma_p)^2} \tag{6}$$

where, j is the imaginary part of the function; ε and σ is the absolute permittivity and conductivity, respectively. The subscripts p and m denote the particle and the medium, respectively. ε_0 is the vacuum dielectric constant ($\varepsilon_0 \approx 8.85\times10^{-12}$ F/m). Equation (2) shows that:

1) The F_{DEP} received by the microparticle is proportional to the third power of the radius of the microparticle. Therefore, microparticles of different sizes will be subjected to F_{DEP} of different sizes due to their different sizes.

2) The size of the F_{DEP} on the microparticles has a positive correlation to the dielectric constant of the air medium.

3) F_{DEP} received by the microparticles is proportional to the square of the electric field intensity gradient. Therefore, by designing the shape of the electrode to increase the gradient of the electric field intensity, the dielectrophoretic force received by the microparticles can be increased.

4) Because the sign of the real part of the CM factor determines the direction of the F_{DEP}. Therefore, the direction of the microparticles subjected to the dielectrophoretic force depends on the electrical conductivity, dielectric constant and alternating current frequency of the microparticles and the air medium. Because the dielectric constant of air is equal to 1, and the conductivity is equal to 0, $\operatorname{Re}[K^*(\omega)]$ is approximately equal to 1. Therefore, the microparticles will be subjected to the positive DEP force (pDEP), that is, the microparticles will move to the area with high electric field intensity.

The analysis of the F_{DEP} on the microparticles in the AC electric field shows that the microparticles will receive the pDEP when they move in the gas. When different types of microparticles are separated by F_{DEP}, the separation can be achieved according to the size of the microparticles and the magnitude of the dielectrophoretic force received.

When manipulating the microparticles in the microfluid, due to the low volume concentration of the microparticles, and the size of the microparticles is much smaller than the characteristic size of the chip, the force between the microparticles and the reaction force of the microparticles on the flow field can be ignored. Therefore, the force of the microparticles in the microfluid by the fluid mainly includes stokes force, Basset force, buoyancy force and additional mass force. Because the microparticles in the microfluid are basically suspended, the buoyancy is almost equal to gravity. Therefore, according to the actual situation, the influence of gravity and buoyancy is ignored, and the influence of the inertial force of the movement of the microparticle on the manipulation of the microparticle is ignored. Therefore, only the stokes force is considered in the fluid force on the microparticles.

In this study, a micropump was used to push the microfluidic gas and microfluid into the microchannel through pressure drive. It is assumed that the speed of fluid flow is stable and the speed of microparticles is relatively small. Particles in a pressure drive flow experience a hydrodynamic drag force expressed as,

$$F_{\text{st}} = 6\pi\mu r(V_m - V_p) \tag{7}$$

where, μ is the dynamic viscosity of the fluid. V_m (m/s) and V_p (m/s) refer to the velocity of the medium and particle, respectively. The direction of the vector difference between the velocity of the microfluid and the velocity of the microparticle determines the direction in which the microparticle receives the Stokes force F_{st}.

In this study, a single shell model was used instead of disease spores[19]. First, the simplest modeling is the single-shell model[29], whose effective dielectric constant is ε^*_{spore}.

$$\varepsilon^*_{spore} = \frac{C^*_{mem} r \varepsilon^*_c}{C^*_{mem} r + \varepsilon^*_c} \tag{8}$$

where, the C^*_{mem} and ε^*_c respectively denote the complex mem-brane capacitance and the complex permittivity of the spore, given by

$$C^*_{mem} = C_{mem} + \frac{g_{mem}}{j\omega} \tag{9}$$

$$\varepsilon^*_c = \varepsilon_c - j\frac{\sigma_c}{\omega} \tag{10}$$

where, C_{mem}, g_{mem}, ε_c and σ_c are the membrane capacitance and conductance per unit area, the spore permittivity and conductivity, respectively. The typical values of these parameters can be found in early publications[30].

2.2 Two-dimensional simulation model of chip

In order to achieve efficient separation and enrichment of greenhouse crops airborne disease spore. Design a two-stage separation-enrichment structure microfluidic chip with the compound field. The two-dimensional diagram of the microfluidic chip is shown in Figure 1. The first structure includes particles entrance, channel 1, arc structure and channel 2. The second structure includes channel 3, channel 4, channel 5, semicircular electrode structure, collection tank and particle exit. R_1 is the radius of arc channels. R_2 is the radius of the collection tank. R_3 is the radius of the semicircular electrode. θ_1 and θ_2 are the separation angles of the particle channels, respectively. The width of channel 1 was set at L_1=2000 μm, length of channel 1= 11 000 μm, R_1=1000 μm, width of arc channel 1=2000 μm, length of channel 2 = 4700 μm, the width of channel 2 was set L_2 = 1500 μm, length of channel 3a and channel 3b=9000 μm, the width of channel 3a and channel 3b were set L_3=2000 μm, length of channel 4a, channel 4b, channel 4c and channel 4d=2300 μm, the width of channel 4a, channel 4b, channel 4c and channel 4d were set L_4=1500 μm, length of channel 5a, channel 5b, channel 5c and channel 5d=2000 μm, the width of channel 5a, channel 5b, channel 5c and channel 5d were set L_5=650 μm, R_2=1000 μm. The height of the microchannel is 100 μm. The range of θ_1 and θ_2 is 10°-40°.

In this study, the finite element analysis software COMSOL Multiphysics 5.1 was used for simulation analysis. The laminar flow module, AC/DC module, and particle trajectory tracking module in the software were used to simulate the separation process. Particle Trajectory Tracking Module coupling the influence of the flow field and electric field on the particle trajectory was used to calculate the trajectory of the particles in the channel.

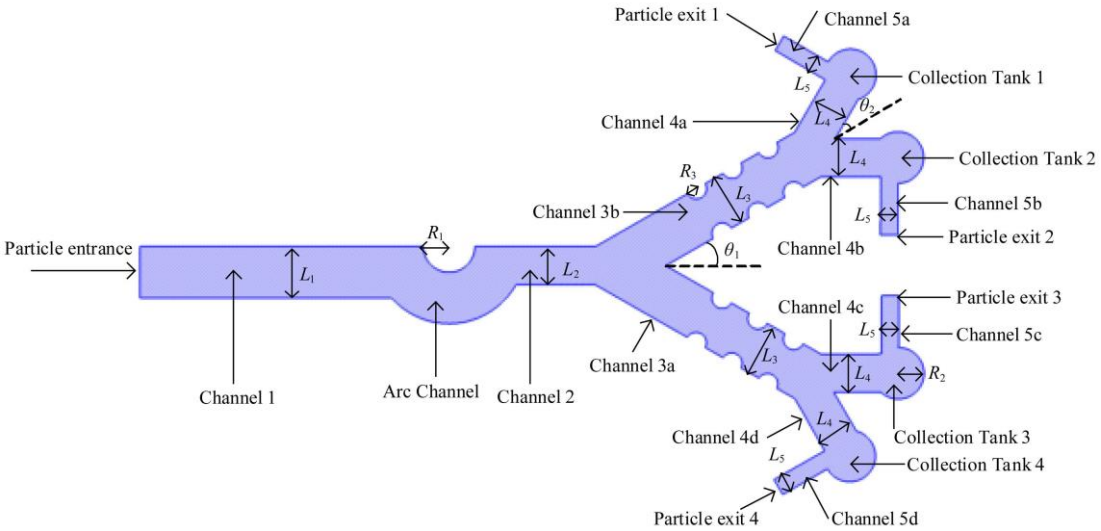

Note: L_1 is the width of channel 1; L_2 is the width of channel 2; L_3 is the width of channel 3a and channel 3b; L_4 is the width of channel 4a, channel 4b, channel 4c and channel 4d; L_5 is the width of channel 5a, channel 5b, channel 5c and channel 5d; R_1 and R_3 are the radii of arc; R_2 is the radius of collection tank 1, collection tank 2, collection tank 3 and collection tank 4.

Figure 1 Two-dimensional diagram of microfluidic chip

2.3 Numerical simulation methods and boundary conditions

The flow field and electric field distribution in the channel were solved in the laminar flow module and the AC/DC module. Laminar flow corresponds to the flow with small Re (Re<1), the viscosity term of the Navier–Stokes equation dominates and the inertia term can be ignored. At this point, Conditions are 1) The channel wall is a non-slip boundary; 2) Flow rates of the inlet is 16 mL/min; 3) Pressure at the outlet is set to be atmospheric pressure, that is $p = 0$. The flow was assumed to be steady, two-dimensional axisymmetric, and incompressible. The temperature was 293.15 K and the applied pressure was 101.3 kPa. The wall was set to adhere. The particle density was set at 1050 kg/m^3. And 100 particles were released from the particle entrance.

A particle tracking module was used in COMSOL 5.1. The dielectrophoretic force and the Stokes force applied to the particles were obtained by solving the electric field and the flow field, respectively. The governing equations for F_{DEP} are given in Equations (2)-(6). At the same time, the single-shell model was used for spore particles, and the governing equation was given by Equation (8). At this point, the corresponding boundary conditions are 1) The channel wall condition is rebound; 2) The initial velocity of the inlet fluid is based on the velocity field in the laminar flow; 3) The drag force follows Stokes' law. Using post-processing in COMSOL 5.1, select the global calculation in the derived value. Data set select the particles to be released, and the expression is the total number of particles in the selection. Count the particles collected in the collection tank area. The

enrichment efficiency of particles was obtained.

2.4 Spore sample preparation

B. cinerea spores, *P. cubensis* spores, and *P. xanthii* spores were collected from the plants' leaves in the Greenhouse of the Key Laboratory of Modern Agricultural Equipment and Technology, Ministry of Education, Jiangsu University, Zhenjiang, Jiangsu, China. Disease spores were inoculated on PDA medium. Propagation was performed on plant leaves when necessary. The morphology of spores was observed under an ultra-deep, three-dimensional microscope (VHX-900F, made by KEYENCE Co., Osaka, Japan)[31]. The measurement results are shown in Table 1.

Table 1 Spore size of three greenhouse crops airborne disease

Species	Spore size/μm×μm
P. xanthii	35.4 (30.2-39.5) ×14.2 (7.3-22.2)
P. cubensis	30.6(21.1-39.8) ×20.5(13.8-23.6)
B. cinerea	19.3(11.4-26.7) ×11.7(8.3-14.5)

The spores in the air are mainly ungerminated spores[32]. Therefore, 30 μm particles were used to represent *P. xanthii* spores, 25 μm particles were used to represent *P. cubensis* spores, and 16 μm particles were used to represent *B. cinerea* spores. less than 10 μm particles were used to represent impurities in the environment.

2.5 Evaluation of airborne disease spore collection efficiency

The collection efficiency of particles can be defined as[33]

$$\eta = \frac{\eta_i}{\eta_i + \eta_j} \times 100\% \tag{11}$$

where, η_i is the number of given particle size spores that pass through the chip and enter the collection tank; η_j is the sum of the number of given particle size spores in the wall of the microchannel in the chip, at each outlet position and in other collection tanks.

3 Results and discussion

3.1 Particle motion simulation

When the particles pass through channel 1 and the arc-shaped channel 1, the force acting on the particles is the same, but the direction of the force is different. The original separation of particles can be achieved. More than 25 μm particles enter channel 3a due to their larger velocity. When the gas passes through the separation angle θ_1, the direction and velocity of the gas flow will change in channel 3a and channel 3b. The speed measured inside the channel is greater than the speed outside. The particles in channel 3a and channel 3b are further separated under different gas velocities, gas directions, θ_2 and $F_{DEP.}$ The 30 μm particles and 16 μm particles enter collection tank 4 and collection tank 1, respectively. The 25 μm particles and less than 10 μm particles enter collection tank 3 and collection tank 2, respectively. In order to achieve this goal, the values of θ_1 and θ_2 need to be numerically simulated. When θ_1 and θ_2 take different values, the enrichment results of particles are shown in Figure 2.

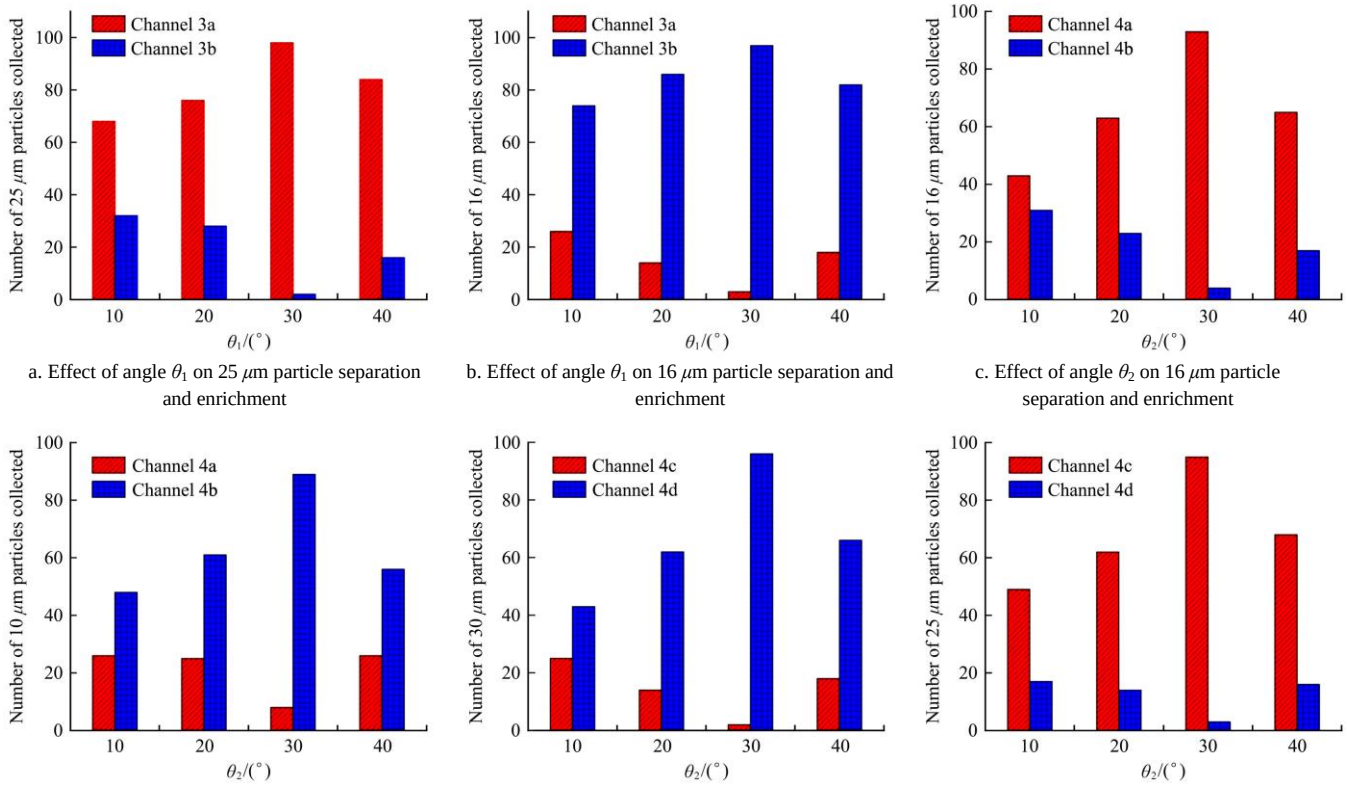

a. Effect of angle θ_1 on 25 μm particle separation and enrichment

b. Effect of angle θ_1 on 16 μm particle separation and enrichment

c. Effect of angle θ_2 on 16 μm particle separation and enrichment

d. Effect of angle θ_2 on 10 μm particle separation and enrichment

e. Effect of angle θ_2 on 30 μm particle separation and enrichment

f. Effect of angle θ_2 on 25 μm particle separation and enrichment

Figure 2 Effects of angle θ_1 and θ_2 on particle separation and enrichment

It can be seen from Figure 2 that when θ_1 and θ_2 are 30°, the separation and enrichment efficiency of particles is relatively high. Therefore, set θ_1 and θ_2 at 30° for the next step of numerical simulation in this study. Because the dielectric constant of air is equal to 1, and the conductivity is equal to 0[34]. It can be seen from Equation (6), Re[$K^*(\omega)$] is approximately equal to 1. According to Equation (2), F_{DEP} on the particle is related to the characteristics of the particle and the electrode voltage. The electrode voltage was set to 120 V, at the frequency of 10^6 Hz[35]. Figures 3a-3d are the simulation results of four kinds of particles. Figure 3e is the intensity of pressure distribution in the microfluidic of the chip. Figure 3f is the velocity distribution in the microchannel of the chip.

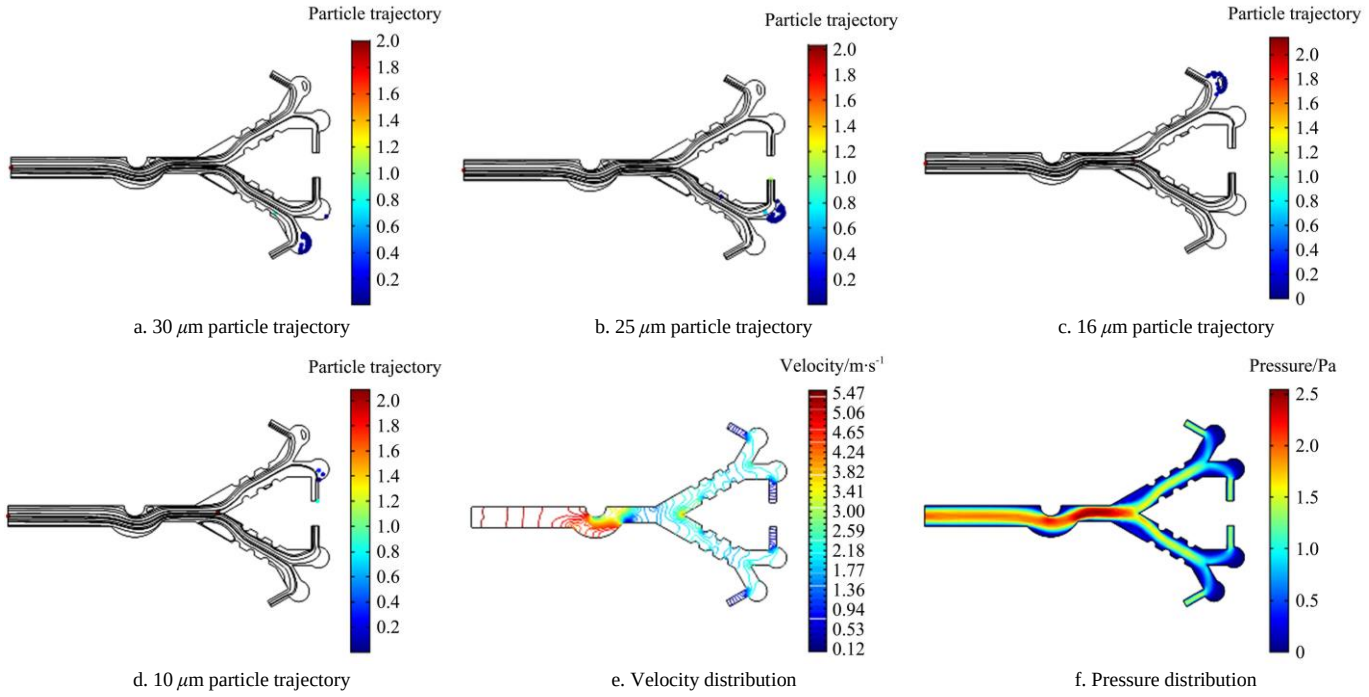

a. 30 μm particle trajectory b. 25 μm particle trajectory c. 16 μm particle trajectory

d. 10 μm particle trajectory e. Velocity distribution f. Pressure distribution

Figure 3 Simulation results of microfluidic chip

As shown in Figure 3, gas enters the microchannel from the particles entrance and obtains a horizontal to right initial velocity[14,15]. The particles enter channel 3a and channel 3b under the action of centrifugal force. When the arc channel is added, the arc channel has a coupling effect with the θ_1 angle turn, which increases the centrifugal force of the particles, so that it can enter channel 3a and channel 3b. The density of all the particles is the same, so the larger the diameter of the particles, the greater the centrifugal force. More than 25 μm particles can enter channel 3a, while less than 16 μm particles can enter channel 3b. When the gas passes through the separation angle θ_1, the direction and velocity of the gas flow will change in channel 3a and channel 3b. The particles in channel 3a and channel 3b were further separated under different gas velocities, gas directions, the separation angle θ_2 and F_{DEP}. The 16 μm particles and 30 μm particles enter collection tank 1 and collection tank 4, respectively. The 10 μm particles and less than 25 μm particles enter collection tank 2 and collection tank 3, respectively. In order to calculate the enrichment results of the particles, four kinds of particles were released from the particles entrance, respectively. The statistical results of particle enrichment are shown in Figure 4.

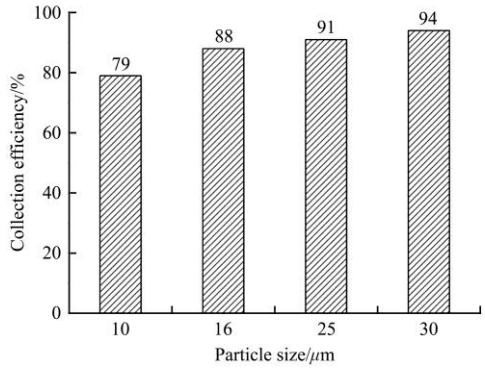

Figure 4 Statistical results of particle enrichment

As can be seen from Figure 4, separation and enrichment efficiency of 10 μm particles, 16 μm particles, 25 μm particles and 30 μm particles was 79%, 88%, 91% and 94%, respectively. The enrichment efficiency of 30 μm particles was highest. The enrichment efficiency of 10 μm particles was low. Because 10 μm particles have a smaller diameter and smaller inertia when the density is constant, and they flow out from the particle exit 2 as the gas flows out[36].

3.2 Experimental verification

The schematic diagram of the experimental platform is shown in Figure 5, including the aerosol generator, the microfluidic device, the dielectrophoretic force generation system and the measurement system.

Airborne disease spore suspension from greenhouse crops was placed in aerosol generators to maintain the integrity and biological activity of spores at low pressure. The compressed air was filtered with HEPA (High efficiency particulate air) to produce a bioaerosol at 2 atmospheres. Place a diffusion dryer behind the aerosol generator (24 Jet Collison, BGI Collison) to remove moisture from the aerosol stream. A ^{210}Po aerosol neutralizer was installed behind the diffusion dryer to remove the charge from the spores[14]. The flow rate of the rotameter (Range of rotameter is 6-60 mL/min) is set to 16 mL/min. Finally, the PDMS layer of the microfluidic chip was removed to expose the collected spores, so the collected greenhouse crop airborne disease spores can be observed by the inverted microscope.

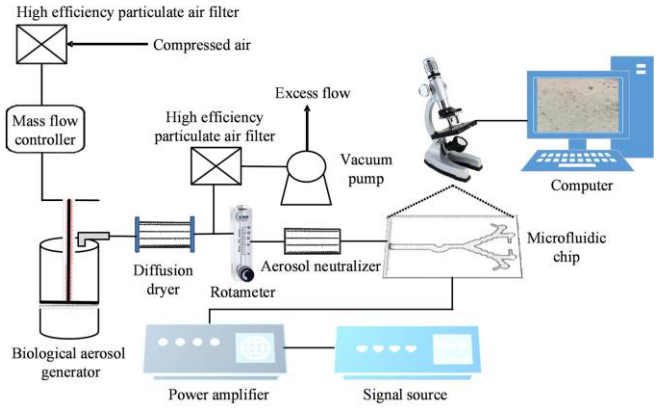

Figure 5 Schematic diagram of the experimental platform

Figure 6 is an experimental image taken by the inverted microscope. *B. cinereal* spores, *P. cubensis* spores and *P. xanthii* spores were collected in collection tank 1, collection tank 3 and collection tank 4, respectively. Therefore, the designed microfluidic chip can separate and collect greenhouse crop airborne disease spores.

The above experiments were carried out for 2 min and repeated five times. And the collected data were analyzed and summarized. The results are shown in Table 2. As can be seen from Table 2, collection efficiency of *B. cinereal* spores, *P. cubensis* spores and *P. xanthii* spores were 75.7%, 83.8% and 89.4%, respectively. Therefore, the proposed microfluidic chip can realize the greenhouse crops airborne disease spore separation and enrichment, which can provide a basis for the research of real-time monitoring technology for greenhouse airborne diseases.

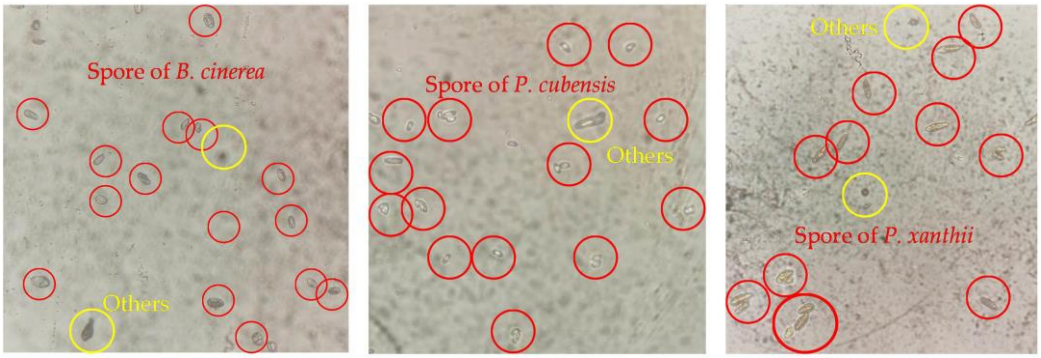

a. *B. cinereal* spores b. *P. cubensis* spores c. *P. xanthii* spores

Figure 6 Experimental results of spores separation and enrichment

Table 2 Statistics results of spore separation-enrichment

Spores	Count type	Experimental groups					
		Group 1	Group 2	Group 3	Group 4	Group 5	Average
B. cinerea	Collection Tank 1	468	506	443	581	457	491
	Other areas	168	165	159	147	151	158
	Sum	636	671	602	608	608	649
	Collection Efficiency	75.7%					
P. cubensis	Collection Tank 3	521	489	574	563	538	537
	Other areas	102	95	112	107	104	104
	Sum	623	584	686	670	642	641
	Collection Efficiency	83.8%					
P. xanthii	Collection Tank 4	462	487	507	473	486	483
	Other areas	57	63	69	46	50	57
	Sum	519	550	576	519	536	540
	Collection Efficiency	89.4%					

4 Conclusions

In this study, in order to realize early monitoring of crop diseases, a two-stage separation-enrichment structure microfluidic chip with a compound field for separation and enrichment the greenhouse crops airborne disease spores directly from gas flow was developed. The chip is mainly composed of three parts: arc structure pretreatment channel, semicircular electrode structure and collection tank. The microfluidic chip was simulated by using COMSOL 5.1 software. The simulation results showed that the separation and enrichment efficiency of 16 μm particles, 25 μm particles and 30 μm particles was 88%, 91% and 94%, respectively. The experimental verification results were observed under a microscope. The results showed that separation and enrichment efficiency of *B. cinereal* spores, *P. cubensis* spores and *P. xanthii* spores were 75.7%, 83.8% and 89.4%, respectively.

Acknowledgements

This work was partially supported by the National Natural Science Foundation of China (Grant No. 32071905; No. 61771224).

[References]

[1] Wang T Y, Wu G X, Chen J W, Cui P, Chen Z X, Yan Y Y, et al. Integration of solar technology to modern greenhouse in China: Current status, challenges and prospect. Renewable & Sustainable Energy Reviews, 2017; 70: 1178–1188.

[2] Wang Y F, Ma G X, Du X X, Liu Y, Wang B, Xu G L, Mao H P. Effects of Nutrient Solution Irrigation Quantity and Downy Mildew Infection on Growth and Physiological Traits of Greenhouse Cucumber. Agronomy, 2020; 10(12): 1921. doi: 10.3390/agronomy10121921.

[3] Hafez Y M, Attia K A, Kamel S, Alamery S F, El-Gendy S, Al-Doss A A, et al. Bacillus subtilis as a bio-agent combined with nano molecules can control powdery mildew disease through histochemical and physiobiochemical changes in cucumber plants. Physiological and Molecular Plant Pathology, 2020; 111: 101489. doi: 10.1016/j.pmpp.2020.101489.

[4] Tanaka K, Fukuda M, Amaki Y, Sakaguchi T, Inai K, Ishihara A, et al. Importance of prumycin produced by Bacillus amyloliquefaciens SD-32 in biocontrol against cucumber powdery mildew disease. Pest management science, 2017; 73: 2419–2428.

[5] Wallace E C, D'Arcangelo K N, Quesada-Ocampo L M. Population analyses reveal two host-adapted clades of *Pseudoperonospora cubensis*, the causal agent of cucurbit downy mildew, on commercial and wild cucurbits. Phytopathology, 2020; 110(9): 1578–1587.

[6] Akhmadeev A A, Salakhov M K. A new approach of recognition of ellipsoidal micro- and nanoparticles on AFM images and determination of

their sizes. Measurement Science and Technology, 2016; 27(10): 105402. doi: 10.1088/0957-0233/27/10/105402.

[7] Lei Y, Yao Z F, He D J. Automatic detection and counting of urediniospores of *Puccinia striiformis* f. sp. *tritici* using spore traps and image processing. Scientific reports, 2018; 8:13647. doi: 10.1038/s41598-018-31899-0.

[8] Chan B D, Icoz K, Huang W F, Chang C L, Savran C A. On-demand weighing of single dry biological particles over a 5-order-of-magnitude dynamic range. Lab on a Chip, 2014; 14(21): 4188–4196.

[9] Sireesha Y, Velazhahan R. Rapid and specific detection of Peronosclerospora sorghi in maize seeds by conventional and real-time PCR. European Journal of Plant Pathology, 2018; 150(2): 521–526.

[10] Bandamaravuri K B, Nayak A K, Bandamaravuri A S, Samad A. Simultaneous detection of downy mildew and powdery mildew pathogens on *Cucumis sativus* and other cucurbits using duplex-qPCR and HRM analysis. AMB Express, 2020; 10(1): 135. doi: 10.1186/s13568-020-01071-x.

[11] Wada M, Tsukada M, Namiki N, Szymanski W W, Noda N, Makino H, et al. A two-stage virtual impactor for in-stack sampling of PM2.5 and PM10 in flue gas of stationary sources. Aerosol and Air Quality Research, 2016; 16(1): 36–45.

[12] Djoumi L, Vanotti M, Blondeau-Patissier V. Real time cascade impactor based on surface acoustic wave delay lines for PM10 and PM2.5 mass concentration measurement. Sensors, 2018; 18(1): 255. doi: 10.3390/s18010255.

[13] Siani O Z, Targhi M Z, Sojoodi M, Movahedin M. Dielectrophoretic separation of monocytes from cancer cells in a microfluidic chip using electrode pitch optimization. Bioprocess and Biosystems Engineering, 2020; 43(9):1573–1586.

[14] Wang P, Yuan S Q, Yang N, Wang A Y, Fordjour A, Chen S B. The Collection method for crop fungal spores based on an efficient microfluidic device. Aerosol and Air Quality Research, 2020; 20(1): 72–79.

[15] Yang N, Chen C Y, Li T, Li Z, Zou L R, Zhang R B, et al. Portable rice disease spores capture and detection method using diffraction fingerprints on microfluidic chip. Micromachines, 2019; 10(5): 289. doi: 10.3390/mi10050289.

[16] Ren Q L, Liang C X, Wang Z X, Qu Z G. Continuous trapping of bacteria in non-Newtonian blood flow using negative dielectrophoresis with quadrupole electrodes. Journal of Physics D-applied Physics, 2021; 54(1): 015401. doi: 10.1088/1361-6463/abb726.

[17] Abd Rahman N, Ibrahim F, Yafouz B. Dielectrophoresis for biomedical sciences applications: A review. Sensors, 2017; 17(3): 449. doi: 10.3390/s17030449.

[18] Ettehad H M, Zarrin P S, Holzel R, Wenger C. Dielectrophoretic immobilization of yeast cells using CMOS integrated microfluidics. micromachines, 2020; 11(5): 501. doi: 10.3390/mi11050501.

[19] Zhang Y L, Chen X Y. Blood cells separation microfluidic chip based on dielectrophoretic force. Journal of the Brazilian Society of Mechanical Sciences and Engineering, 2020; 42(4): 206. doi: 10.1007/s40430-020-02284-8.

[20] Zhang Y, Wang S Y, Chen J, Yang F, Li G Y. Separation of macrophages using a dielectrophoresis-based microfluidic device. Biochip Journal, 2020; 14(2): 185–194.

[21] Lee K, Lee J, Ha D, Kim M, Kim T. Low-electric-potential-assisted diffusiophoresis for continuous separation of nanoparticles on a chip. Lab on a Chip, 2020; 20(15): 2735–2747.

[22] Tajik P, Saidi M S, Kashaninejad N, Nguyen N T. Simple, cost-effective, and continuous 3D dielectrophoretic microchip for concentration and separation of bioparticles. Industrial & Engineering Chemistry Research, 2020; 59(9): 3772–3783.

[23] Natu R, Martinez-Duarte R. Numerical model of streaming DEP for stem cell sorting. Micromachines, 2016; 7(12): 217. doi: 10.3390/mi7120217.

[24] Ayala-Mar S, Perez-Gonzalez V H, Mata-Gomez M A, Gallo-Villanueva R C, Gonzalez-Valdez J. Electrokinetically driven exosome separation and concentration using dielectrophoretic-enhanced PDMS-based microfluidics. Analytical Chemistry, 2019; 91(23): 14975–14982.

[25] Hirota Y, Hakoda M, Wakizaka Y. Separation characteristics of animal cells using a dielectrophoretic filter. Bioprocess and Biosystems Engineering, 2010; 33(5): 607–612.

[26] Han S I, Huang C, Han A. In-droplet cell separation based on bipolar dielectrophoretic response to facilitate cellular droplet assays. Lab on a Chip, 2020; 20(20): 3832–3841.

[27] Gascoyne P R C, Shim S, Noshari J, Becker F F, Stemke-Hale K. Correlations between the dielectric properties and exterior morphology of cells revealed by dielectrophoretic field-flow fractionation. Electrophoresis, 2013; 34(7): 1042–1050.

[28] Chen L, Liu X, Zheng X L, Zhang X L, Yang J, Tian T, et al. Dielectrophoretic separation of particles using microfluidic chip with composite three-dimensional electrode. Micromachines, 2020; 11(7): 700. doi: 10.3390/mi11070700.

[29] Alnaimat F, Mathew B, Hilal-Alnaqbi A. Modeling a dielectrophoretic microfluidic device with vertical interdigitated transducer electrodes for separation of microparticles based on size. Micromachines, 2020; 11(6): 563. doi: 10.3390/mi11060563.

[30] Zhang Z L, Luo Y, Nie X F, Yu D L, Xing X X. A one-step molded microfluidic chip featuring a two-layer silver-PDMS microelectrode for dielectrophoretic cell separation. Analyst, 2020; 145(16): 5603–5614.

[31] Wang Y F, Du X X, Ma G X, Liu Y, Wang B, Mao H P. Classification methods for airborne disease spores from greenhouse crops based on multifeature fusion. Applied Science, 2020; 10(21): 7850. doi: 10.3390/app10217850.

[32] Zhu Y D, Zhang J Y, Li M Y, Zhao L J, Ren H R, Yan L G, et al. Rapid determination of spore germinability of *Clostridium perfringens* based on microscopic hyperspectral imaging technology and chemometrics. Journal of Food Engineering, 2020; 280: 109896. doi: 10.1016/j.foodeng.2019.109896.

[33] Xu P F, Zhang R B, Yang N, Oppong P K, Sun J. High-precision extraction and concentration detection of airborne disease microorganisms based on microfluidic chip. Biomicrofluidics, 2019; 13(2): 024110. doi: 10.1063/1.5086087.

[34] Tian E Z, Xia F X, Wu J D, Zhang Y P, Li J, Wang H, et al. Electrostatic air filtration by multifunctional dielectric heterocaking filters with ultralow pressure drop. Acs Applied Materials & Interfaces, 2020; 12(26): 29383–29392.

[35] Shi L Y, Shi X M, Zhou T, Liu Z Y, Liu Z Y, Joo S. A full-scale computational study on the electrodynamics of a rigid particle in an optically induced dielectrophoresis chip. Modern Physics Letters B, 2020; 34(22): 2050233. doi: 10.1142/S0217984920502334.

[36] Ho M T, Li J, Su W, Wu L, Borg M K, Li Z H, et al. Rarefied flow separation in microchannel with bends. Journal of Fluid Mechanics, 2020; 901: A26. doi: 10.1017/jfm.2020.585.